Chapter 2
Experimental Study on the Nanofluid Dynamic Wetting

Abstract In this chapter, the time-dependent wetting radius and contact angle for various nanofluid droplets were measured to study the dynamic wetting behaviors of nanofluids. The experiment results show that the adding of nanoparticles inhibits the dynamic wetting of nanofluids as compared with base fluids. The reduced spreading rate can be attributed to the increase in either surface tension or viscosity due to adding nanoparticles into the base fluid. Once the effects of the surfaces tension and viscosity are both eliminated using the non-dimensional analysis, the wetting radius versus spreading time curves for all the nanofluid droplets overlap with each other. The spreading exponent fitted from the nanofluid dynamic wetting data agrees with the prediction of the classical hydrodynamics model derived from the bulk viscous dissipation approach. The present study proves that the spreading of the nanofluid droplets is dominated by the bulk dissipation rather than by the local dissipation at the moving contact line.

2.1 Introduction

The attractive and tunable wetting behaviors extend the applications of nanofluids into many scientific and engineering areas; however, the mechanisms of nanofluid dynamic wetting are not well understood [1–6]. Many parameters may be controlled in nanofluids, such as the nanoparticle material, size, shape, and loading, as well as base fluid material. By changing nanoparticles or base fluid, nanofluids exhibit enhanced [3] or reduced [7] thermal conductivity, increased [8, 9] or decreased [10] surface tension, as well as shear-thinning [11] or shear-thickening [12] rheological properties. It can be expected that when nanofluid droplets spread on a solid surface, they will also show different dynamic wetting behaviors. The expectation has been confirmed by the recent reports [13–18]. Wang et al. [13, 14] compared experimentally the spreading behaviors of pure poly (propylene glycol, PPG) and PPG+10 nm silica nanofluids. Their results showed that the wetting radius versus time relation ($R - t$) and the dynamic contact angle versus contact line

G. Lu, *Dynamic Wetting by Nanofluids*,
Springer Theses, DOI 10.1007/978-3-662-48765-5_2

velocity relation ($\theta_D - U$) for the pure PPG followed the Newtonian spreading laws; however, the $R - t$ and $\theta_D - U$ relations for the PPG+ silica nanofluids significantly deviated from the Newtonian spreading laws. The deviations were attributed to the fact that adding silica nanoparticles into the solvent led to a shear-thickening rheology. However, a distinct dynamic wetting behavior for nanofluids was reported by Wasan et al. [15–18]. They presented that 8 nm micellar solution and 20-nm silica suspension significantly enhanced the spreading rate as compared with their base fluids. A solid-like ordering structure of nanoparticles was observed near the contact line region using interferometry [15]. Thus, the super-spreading was explained by the structural disjoining pressure due to the self-assembly of nanoparticles in the vicinity of the contact line [15–18]. The super-spreading behavior of nanofluids has been widely used to explain the enhanced drop-wise evaporation [19, 20] and the elevated critical heat flux with nanofluids [21–24]. Another explanation for the super-spreading by nanofluids was that nanoparticles were assumed to settle at the bottom of the droplet, thus reducing the solid–liquid friction and hence facilitating the fluid spreading [25].

The previous studies [13–18] dealt with dynamic wetting behaviors of nanofluids with high nanoparticles fraction. However, high fraction nanofluids are unstable due to the nanoparticle sedimentation, which has become a serious challenge for potential applications of nanofluids. Thus, it is indeed necessary to investigate dynamic wetting characteristics of dilute nanofluids. Recently, Liang et al. [26] proposed that the timescale for the nanoparticles diffusing from the bulk droplet to the contact line region is far larger than that for the droplet spreading, so that the nanoparticle fraction in the contact line region is actually lower than the nominal fraction of bulk droplet. As a result, the shear-thickening nanofluids behave like quasi-Newtonian spreading characteristics. The limited diffusion rate of the nanoparticles was also confirmed for the spreading of gold–water nanofluids on a gold surface via molecular dynamic simulations [27]. For the dilute nanofluids, nanoparticles are harder to diffuse to the contact line region; thus, the super-spreading and shear-thickening spreading may not occur. Unfortunately, the dynamic wetting for the dilute nanofluids has not been reported up to now.

The relations of θ_D–U and R–t are usually used to describe the dynamic wetting of fluids on solid surfaces. These two relations not only present the wettability of the fluids on the solid surfaces, but also show the energy dissipation mechanisms during the dynamic wetting process [28–31]. Unfortunately, few studies focus on measurements of θ_D–U and R–t for nanofluids. Without θ_D–U and R–t experimental data, the dynamic behaviors cannot be accurately described.

This chapter investigates dynamic wetting behaviors of dilute nanofluids by measuring θ_D–U and R–t data using the droplet spreading method. The effects of nanoparticle material, diameter, and loading, as well as base fluid and substrate material, were examined. The purpose of this work is to reach the following two targets. The first is to answer whether the super-spreading and/or shear-thickening spreading behaviors will also be observed for dilute nanofluids. The second is to address how nanoparticles affect dynamic wetting behaviors in dilute nanofluids, if the two behaviors do not occur.

2.2 Experimental Methods

2.2.1 Experimental Setup

The θ_D–U and R–t data were first measured using a drop shape analyzer (EasyDrop FM40, Krüss GmbH, Hamburg, Germany), as shown in Fig. 2.1a. The spreading process was recorded by a high-speed CCD camera at 60 frames per second. The contact angle and the spreading radius were measured by fitting the droplet profile with the equation $y = a + bx + cx^{0.5} + d/\ln x + e/x^2$ for each picture as shown in Fig. 2.1b. The standard error in the contact angle measurement was ±1°. The contact line velocity was calculated using $U = \mathrm{d}f(t)/\mathrm{d}t$, where $f(t)$ was fit from the R–t curves.

The surface tension and the θ_D–U curves were then measured using Krüss K100 MK2 (Krüss GmbH, Hamburg, Germany) based on the Wilhelmy plate method, as shown in Fig. 2.2. The substrate was inserted into the liquid reservoir at various velocities. As shown in Fig. 2.2b, the forces imposed on the plate are as follows:

$$F = L \cdot \sigma \cdot \cos\theta_D - \rho g S h, \tag{2.1}$$

where L is the wetting perimeter, ρ is the liquid density, S is the cross-sectional area of the plate, h is the inserted distance, and γ is the liquid–vapor surface tension. The measured F–h curves had good linearity as shown in Fig. 2.2b with the contact angle and then the contact angle is calculated as follows:

$$\theta_D = \arccos\left(\frac{F_0}{L \cdot \sigma}\right), \tag{2.2}$$

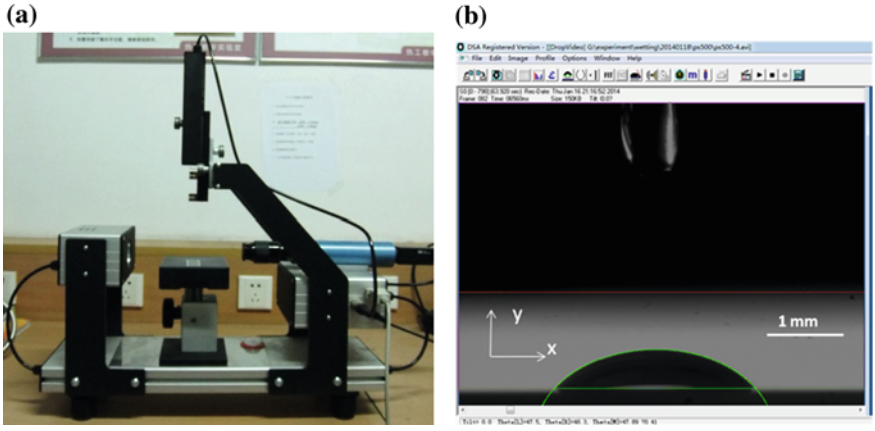

Fig. 2.1 Droplet spreading method: **a** Krüss EasyDrop; **b** Contact angle and spreading radii based on image analysis

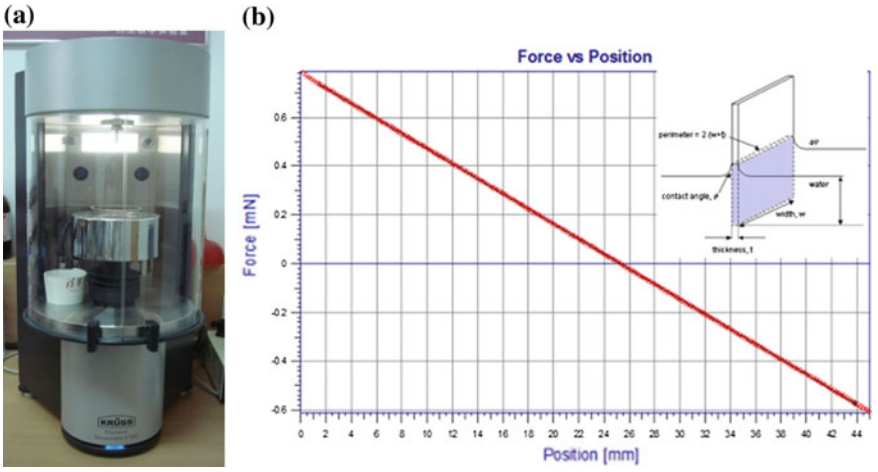

Fig. 2.2 Wilhelmy plate method: **a** Krüss K100 MK2; **b** schematic

Table 2.1 Experimental capacities

Measurement	Method	Company	Type	Capability
$R-t$, θ_D-U	Droplet spreading	Krüss	Krüss FM40 EasyDrop Standard	Resolution: 0.1°; Highest capture spread: 60 frames/s
σ, θ_D-U	Wilhelmy plate	Krüss	Krüss K100 MK2	Max insert: 110 mm; resolution: 0.1 μm; Velocity range: 0.09–500 mm min^{-1}

where F_0 is the intercept in Fig. 2.2b. The surface tension was also measured by a Krüss K100 MK2 using a platinum plate.

The accuracies of the experimental setups are listed in Table 2.1.

2.2.2 *Nanofluid Preparation*

The measurements of the nanofluid dynamic wetting characteristics required stable nanofluids and clean substrates and beakers. Hence, all the substrates (glass slides, mica slides, and silicon wafers) and the beakers were cleaned with ethanol solution with more than 30-min ultrasonic cleaning. The ultrasonic cleaning procedure was then repeated with acetone and then with the deionized water.

As shown in Table 2.2, the study considered the effects of various nanofluid parameters on the dynamic wetting, including the nanoparticle loading (SiO_2/PDMS500 (polydimethylsiloxane, viscosity of 100 mPa s), $d = 20$ nm, $\varphi = 0$, 0.5, 1, and 2 %), nanoparticle material (SiO_2, TiO_2, Al_2O_3/PDMS500, d = 20 nm,

Table 2.2 Nanofluid parameters used for the dynamic wetting tests

Effects	Materials[a]	Diameter (nm)	Base fluids[a]	Loadings (%)	Substrates
Loadings	SiO_2	20	PDMS500	0.5	Glass
	SiO_2	20	PDMS500	1	Glass
	SiO_2	20	PDMS500	2	Glass
Diameters	SiO_2	10	PDMS500	1	Glass
	SiO_2	15	PDMS500	1	Glass
	SiO_2	20	PDMS500	1	Glass
Materials	SiO_2	20	PDMS500	1	Glass
	TiO_2	20	PDMS500	1	Glass
	Al_2O_3	20	PDMS500	1	Glass
Base fluids	SiO_2	10	PDMS100	1	Glass
	SiO_2	10	PDMS500	1	Glass
	SiO_2	10	PDMS1000	1	Glass
	SiO_2	10	PEG200	1	Glass
	SiO_2	10	PEG400	1	Glass
Substrates	SiO_2	20	PDMS500	1	Glass[b]
	SiO_2	20	PDMS500	1	Mica[c]
	SiO_2	20	PDMS500	1	Silicon wafer[d]

[a]Sigma-Aldrich Co., [b]Fisher Co., [c]SPI Supplies, and [d]UMCO

Table 2.3 Nanoparticle properties

Properties	SiO_2	SiO_2	SiO_2	TiO_2	Al_2O_3
Wettability	Hydrophilic				
BET (m^2/g)	90 ± 15	130 ± 25	150 ± 15	50 ± 15	100 ± 15
Diameter (nm)	10 ± 1	15 ± 1	20 ± 1	20 ± 1	20 ± 1
Density (g/l)	50–120	50–120	50–120	–100	–80

φ = 1 %), nanoparticle diameter (SiO_2/PDMS500, φ = 1 %, d = 10, 15, and 20 nm), and base fluid (SiO_2/PDMS100, PDMS500, PDMS1000, PEG200 (polyethylene glycol, molecular weight of 200 g/mol), PEG4000, d = 20 nm, φ = 1 %). All the nanoparticles (SiO_2, TiO_2, and Al_2O_3) and base fluids (PDMS100, PDMS500, PDMS1000, PEG200, and PEG4000) were Sigma-Aldrich products.

Stable nanofluids were obtained by mixing all the nanofluid suspensions in the ultrasonic cleaner for more than 12 h. The nanofluids were observed to be stable for 48 h. All the measurements were conducted within 1 or 2 h after the nanofluids were prepared. In addition, the dynamic wetting attests to a small droplet lasts only several minutes, which is much shorter than the nanofluid stability time. Hence, the nanofluid stability had no effect on the dynamic wetting experiments. All the tested nanofluid parameters and substrates are listed in Table 2.3.

2.2.3 *Experiment Repeatability and Reliability*

The repeatability and reliability of experimental method are illustrated by the details shown in Figs. 2.3, 2.4, and 2.5. Figure 2.3 shows the spreading radius (Fig. 2.3a) and the dynamic contact angle (Fig. 2.3b) evolution for three tests with the same PDMS500 liquid within 1 h after the fluid was prepared. Both the spreading radius and the dynamic contact angle evolution curves almost overlap, indicating the repeatability and reliability of the experimental method. Figure 2.4 shows seven

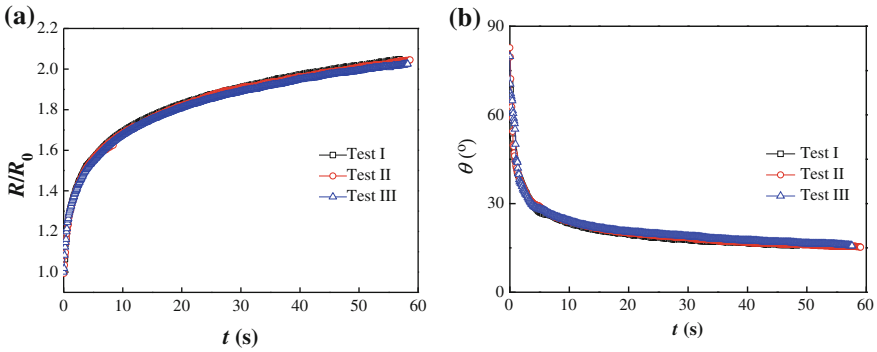

Fig. 2.3 Experiment repeatability testing: three measurements of **a** spreading radius versus time and **b** dynamic contact angle evolutions for the same PDMS500 liquid within 1 h

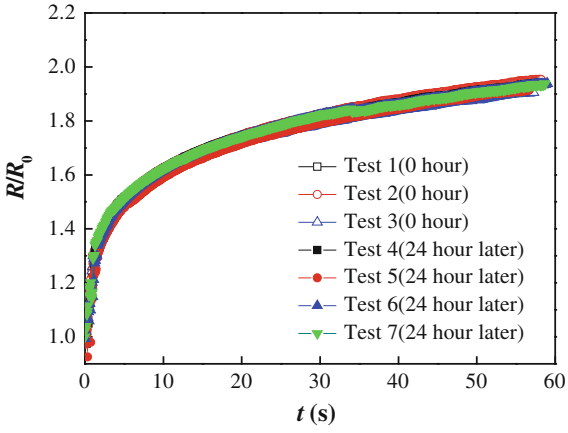

Fig. 2.4 Seven measurements of spreading radius evolution for the same SiO_2/PDMS500 nanofluids (d = 20 nm, φ = 0.5 %): Test Nos. 1–3 were measured immediately when the nanofluids were well prepared; Test Nos. 4–7 were measured after 24 h when the nanofluids were prepared

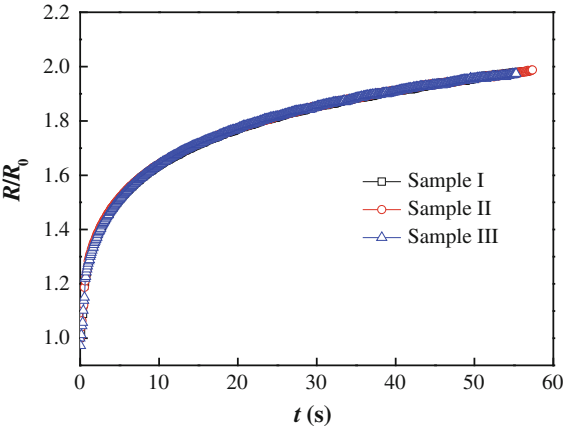

Fig. 2.5 Dynamic wetting measurements of Al_2O_3/PDMS500 nanofluids (d = 20 nm, φ = 0.5 %) which were prepared at different times

measurements for the same SiO_2/PDMS500 nanofluid (d = 20 nm, φ = 0.5 %), in which Test Nos. 1–3 were measured immediately when the nanofluids were prepared, while Test Nos. 4–7 were measured 24 h after the nanofluids were prepared. The consistent results show the good stability of the nanofluids. Figure 2.5 shows the dynamic wetting characteristics of Al_2O_3/PDMS500 nanofluids (d = 20 nm, φ = 0.5 %) prepared at different times. The overlapping curves show the repeatability of the nanofluid preparation method.

2.3 Results and Discussions

2.3.1 Spreading Behavior of Dilute Nanofluids

Figure 2.6 shows the evolution of the spreading radius for SiO_2/PDMS500 nanofluid droplets with various nanoparticle loadings (φ = 0, 0.5, 1, and 2 %) on the glass slide. Here, R_0 denotes the droplet radius prior to spreading. Since glass slides, mica slides, and silicon wafers are high-energy surfaces, the nanofluid droplets studied in this work were found to spread completely to a thin film on these surfaces. Consequently, the initial radius, R_0, was used for the non-dimensional analysis. Compared with the base fluid (φ = 0), adding nanoparticles inhibits rather than facilitates the dynamic wetting for the three nanoparticle loadings (φ = 0.5, 1, and 2 %). The spreading rate and the spreading area decrease with increasing nanoparticle loadings, for example, R/R_0 = 2.10 for PDMS500 (φ = 0) at t = 50 s, while R/R_0 = 1.99 for φ = 0.5 %, R/R_0 = 1.93 for φ = 1 %, and R/R_0 = 1.89 for φ = 2 %. The reduced spreading speed and the equilibrium wetting radius were also reported for the impinging of a liquid drop with micron-sized particles on surfaces [32]. For the micron-sized particles, the sedimentation of particles takes place more easily. Thus, an annular particle distribution was observed for higher impinging

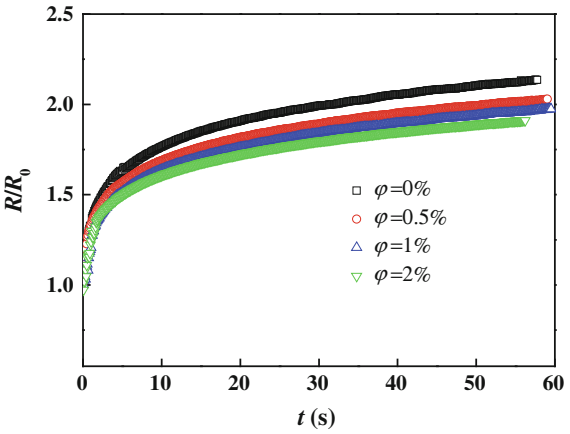

Fig. 2.6 Effects of nanoparticle loadings on the dynamic wetting of nanofluids (SiO_2, PDMS500, φ = 0, 0.5, 1, and 2 %, d = 20 nm)

velocities, and the periphery of the drop was always depleted of particles owing to interfacial forces acting on the particles [32]. However, these phenomena do not occur for the spreading of dilute nanofluids.

2.3.2 *Individual Parameter Analysis of Nanofluid Dynamic Wetting*

To perform the individual parameter analysis, the nanofluids were divided into two groups. One group has different viscosities, while the surface tensions are the same (base fluids: PDMS100, PDMS500, and PDMS1000, nanoparticles: SiO_2 with φ = 1 % and d = 10 nm); the other has different surface tensions, while the viscosities are almost the same (base fluids: PDMS100, PEG200, and PEG400, nanoparticles: SiO_2 with φ = 1 % and d = 10 nm). Therefore, the effects of viscosity and surface tension can be examined individually. The base fluid properties are shown in Table 2.4.

Table 2.4 Base fluid properties at 20 °C

Base fluids	Density (g/mL)	Surface tension (10^{-3} N/m)	Viscosity (10^{-3} Pa s)
PDMS100[a]	1.06	20.0	100
PDMS500	0.97	20.0	500
PDMS1000	1.09	20.0	1000
PEG200[b]	1.12	37.2	108
PEG400	1.12	43.5	120

[a]PDMS100 is polydimethylsiloxane with viscosity of 100 mPa s
[b]PEG200 is polyethylene glycol with molecular weight of 200 g mol^{-1}

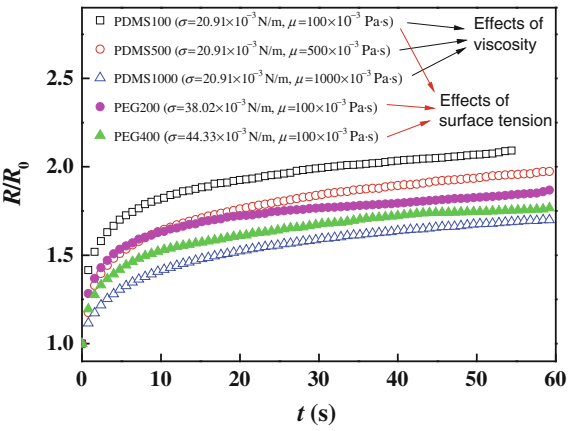

Fig. 2.7 Effects of base fluid materials on nanofluids dynamic wetting (SiO_2, φ = 1 %, d = 10 nm)

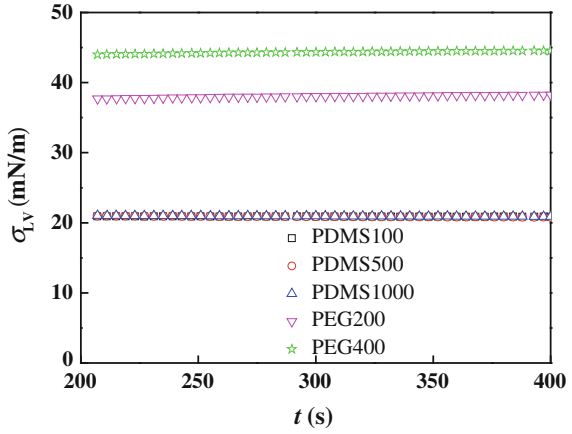

Fig. 2.8 The surface tensions of nanofluids (SiO_2, d = 10 nm, φ = 1 %)

Figure 2.7 shows $(R/R_0) - t$ curves of the five nanofluids. It is found that the viscosity and surface tension strongly affect the nanofluid dynamic wetting. Both the spreading velocity and the spreading area decrease with increasing viscosity for the three PDMS-based nanofluids. For example, R/R_0 is 2.07 for the PDMS100-nanofluid at t = 50 s, while R/R_0 = 1.94 for the PDMS500-nanofluid, and R/R_0 = 1.65 for the PDMS1000-nanofluid. For the nanofluids with the same viscosity (PDMS100-based, PEG200-based, and PEG400-based), the spreading deteriorates with increasing base fluid surface tensions. As shown in Fig. 2.8, the surface tensions of the five nanofluids measured by the Krüss K100 MK2 remain unchanged for a long time (longer than the dynamic spreading process). The surface tension is 20.91 ± 0.04 mN m^{-1} for the three PDMS-based nanofluids, 38.02 ± 0.05 mN m^{-1} for SiO_2/PEG200, and 44.33 ± 0.05 mN m^{-1} for SiO_2/PEG400. The effects of surface tension on the dynamic wetting are explained as follows. The driving force acting on the contact line can be expressed as

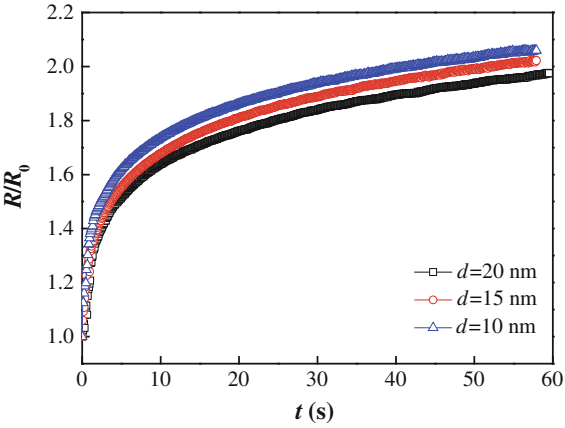

Fig. 2.9 Effects of three nanoparticle diameters on the dynamic wetting (SiO_2/PDMS500, φ = 1 %); inserted schematic: non-dimensional radius versus non-dimensional time

$F = \sigma_{SV} - \sigma_{SL} - \sigma_{LV}\cos\theta_D$, where σ_{SV} and σ_{SL} denote the solid–vapor and solid–liquid interfacial tensions, and σ_{LV} is the liquid–vapor interfacial tension (also referred to as the liquid surface tension). Restated that the nanofluids studied can completely spread on the glass slides, mica slides, and silicon wafers, the dynamic contact angle, θ_D, is always smaller 90° in all spreading experiments. Thus, the increase in σ_{LV} reduces the driving force, which leads to the slower spreading for nanofluids with larger surface tension.

Figure 2.9 shows the effects of the nanoparticle diameter (SiO_2 with d = 10, 15, and 20 nm, the standard deviation of diameter for each nanoparticle is about ±1 nm) on the nanofluid dynamic wetting. The base fluid is PDMS500, and the nanoparticle loading is 1 %. The spreading velocity and spreading area both decrease with increasing nanoparticle diameter. The effects of nanoparticle diameter on the viscosity have been studied experimentally and theoretically [33–36]. These studies demonstrated that increasing the nanoparticle diameter increases the nanofluid viscosity. However, there are no direct evidences to relate the nanoparticle diameter to the surface tension of nanofluids [37–39]. It was reported that the wettability of nanoparticles was responsible for the modified surface tension of nanofluids; adding hydrophilic nanoparticles increases the surface tension of nanofluids, while adding hydrophobic nanoparticles reduces the surface tension [40]. We also measured the surface tensions of nanofluids with the three different nanoparticle diameters. Because the SiO_2 nanoparticles used are hydrophilic, the surface tensions of the three nanofluids are all higher than that of the base fluid, which agrees with the report in Ref. [40]. The results also show that three nanofluids have the same surface tension, indicating that the nanoparticle diameters do not affect the surface tension of nanofluids. Therefore, Fig. 2.9 again confirms that increasing nanofluid viscosity slows down the spreading of nanofluids.

Based on the individual parameter analysis, it is concluded that the super-spreading behavior does not take place, and the viscosity and surface tension are two dominant parameters for the dynamic spreading of dilute nanofluids.

2.3.3 Coupling Effect of Viscosity and Surface Tension

The non-dimensional spreading radius (R/R_0) as a function of the coupling parameter, $t/\mu\sigma_{LV}^2 R_0$, is shown in Fig. 2.10. The use of the coupling parameter is to eliminate the effects of both the surface tension and the viscosity. By eliminating the differences of the surface tension and the viscosity, the original experimental data of R/R_0 versus t (Fig. 2.7) measured for various nanofluids gather together nearly into a single curve. This result indicates that apart from the viscosity and surface tension, there is no other parameter affecting the dynamic wetting of dilute nanofluids. Therefore, for dilute nanofluids, the role of nanoparticles in the dynamic wetting is realized only through modifying the viscosity and surface tension of nanofluids.

The effects of surface tension and viscosity on the dynamic wetting of dilute nanofluids were further tested by adding three different nanoparticle materials (SiO_2, Al_2O_3, and TiO_2) into the same base fluid (PDMS500). The average nanoparticle diameters are 20 nm, and the loadings are 1 % for the three nanoparticle materials. In addition, the three nanoparticles are spherical without any surface treatments. Experimental tests show that three nanofluids have almost the same surface tension and viscosity; thus, R/R_0 versus t curves are expected to coincide with each other. This is verified by the spreading experiments shown in Fig. 2.11.

2.3.4 Mechanisms of Dynamic Wetting in Dilute Nanofluids

2.3.4.1 Spreading Law of Dilute Nanofluids

The R/R_0–t data in Fig. 2.6 were replotted in the dual-logarithmic coordinates, as shown in Fig. 2.12. It is found that the new curves for four nanoparticle loadings are all linear ($R^2 = 0.999$). The curves were then fitted by R–At^{α} with the results listed

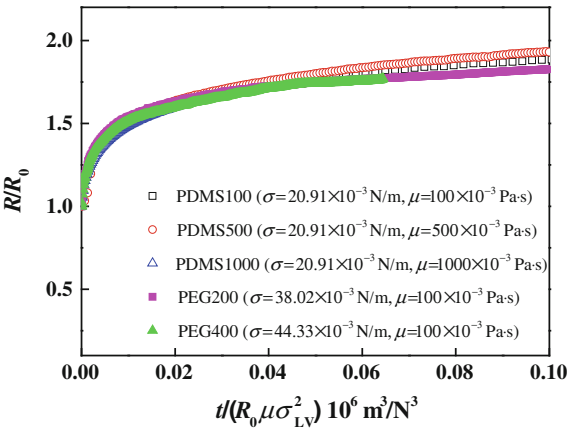

Fig. 2.10 Effects of surface tension and viscosity on the dynamic wetting of nanofluids using non-dimensional analyzing

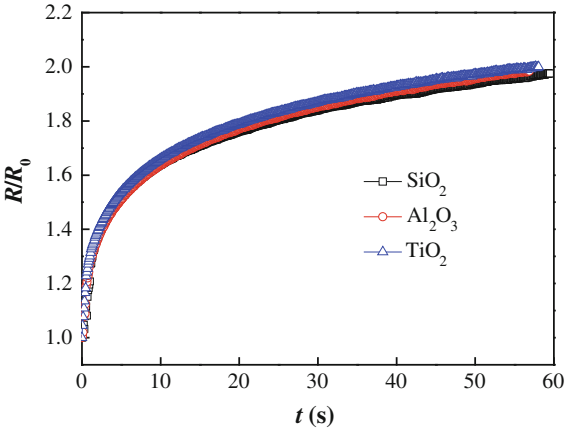

Fig. 2.11 Effects of three nanoparticle materials on the dynamic wetting (PDMS500, φ = 1 %, d = 20 nm)

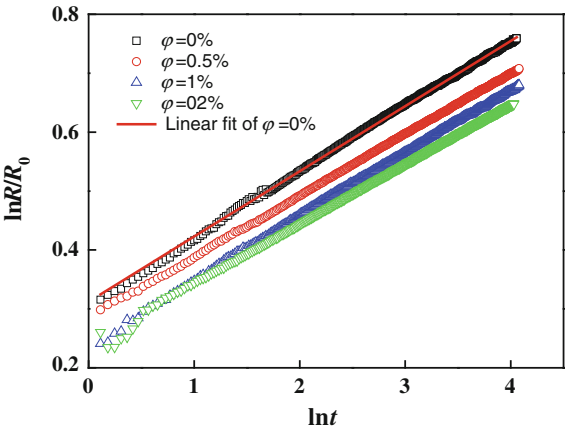

Fig. 2.12 Linear fitting in the logarithmic coordinates for nanofluid dynamic wetting with various nanoparticle loadings (SiO_2, PDMS500, φ = 0, 0.5, 1, and 2 %, d = 20 nm)

in Table 2.5. The spreading exponent, α, can be used to determine the energy dissipation mechanism. If the dynamic wetting is dominated only by the energy dissipation occurred in the vicinity of contact line, referred to as local dissipation, the molecular kinetic theory (MKT) predicts α = 1/7 [31]. On the contrary, the hydrodynamics model [28–30] assumed that the viscous dissipation in the bulk droplet dominates the dynamic wetting, which predicts α = 1/8 in the gravitational spreading regime and α = 1/10 in the capillary spreading regime.

The fitted spreading exponents, α, are close to 1/10 (Δ = 11 % for φ = 0 %, Δ = 4 % for φ = 0.5 %, Δ = 6 % for φ = 1 %, and Δ = 0 % for φ = 0 %), which meets the prediction of the classical hydrodynamics model derived from the bulk viscous dissipation approach for Newtonian flows. Therefore, the bulk dissipation dominates the dynamic wetting of SiO_2/PDMS500 nanofluids. It should be noted that the super-spreading of nanofluids is controlled by the local energy dissipation, because the super-spreading comes from the structural disjoining pressure due to the

Table 2.5 Spreading laws of SiO_2-PDMS500 with various loadings

φ (%)	A	α	R^2
0	1.366	0.111	0.999
0.5	1.329	0.104	0.999
1	1.277	0.106	0.999
2	1.273	0.100	0.998

nanoparticle self-assembly near the contact line region. Thus, the bulk dissipation mechanism for dynamic wetting of dilute nanofluids indicates that the nanoparticles do have no enough time to diffuse to the contact line region during the dynamic wetting so that the self-assembly of nanoparticles cannot take place in the present dilute nanofluids. According to the hydrodynamics model, the spreading exponents of about 1/10 also indicate that the capillary force is the only driving force, while the viscous force is the only resistance force. Thus, the role of adding nanoparticles in dilute nanofluids is to change the viscosity and surface tension of nanofluids, and then, these two physical properties affect the dynamic wetting.

2.3.4.2 Nanoparticle Behaviors During Dilute Nanofluid Dynamic Wetting

Figure 2.13 shows the dynamic wetting of SiO_2/PDMS500 nanofluids (d = 20 nm, φ = 1 %) on glass, silicon, and mica slides. The three substrates are chemically and physically homogeneous. The AFM scanning results show that all three surfaces have nanoscale roughness (the root-mean-square roughness is 0.231 nm for glass slide surface, 0.125 nm for the silicon, and 0.137 nm for the mica), as shown in Fig. 2.14. Therefore, the substrates are smooth and ideal surfaces for dynamic wetting [41], so that the dynamic wetting is only affected by the solid surface energy of these three substrates.

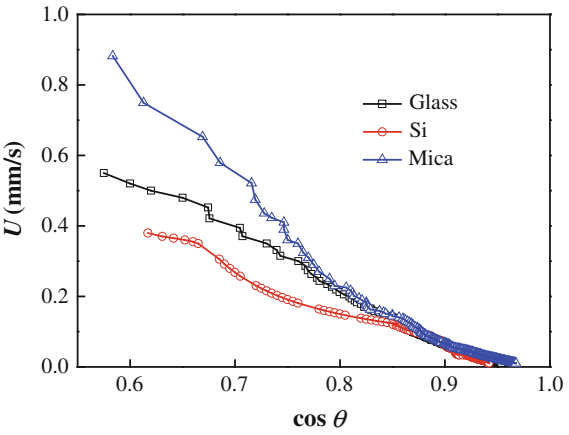

Fig. 2.13 Contact line velocity versus the contact angle for three substrates

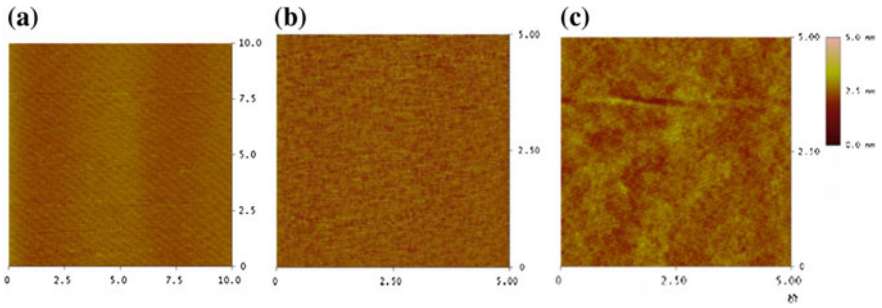

Fig. 2.14 Surface roughness scanning of three substrates using AFM: **a** glass slide; **b** sillicon wafor; **c** mica slide

According to MKT [31], the ratio of the contact line velocity to the cosine of contact angle is proportional to the ratio of the liquid–vapor surface tension and the solid–liquid friction coefficient,

$$U/\cos\theta_{\mathrm{D}} \sim \sigma_{\mathrm{LV}}/\zeta, \tag{2.3}$$

where ζ is the solid–liquid "friction" coefficient in the MKT model, characterizing the intermolecular interactions between the solid substrate and liquid phase. The $U-\cos\theta_{\mathrm{D}}$ curves for the three substrates (Fig. 2.10) are linear over most of the droplet spreading time. The ratios of $\sigma_{\mathrm{LV}}/\zeta$ can be obtained from the slopes of the $U-\cos\theta_{\mathrm{D}}$ curves. With σ_{LV} = 20.91 mN m^{-1} for SiO_2/PDMS500 nanofluids, ζ is 14.95 Pa s for the glass slides, ζ = 19.13 Pa s for the silicon wafer slides, and ζ = 9.03 Pa s for the mica slides. The "friction" coefficient ζ is used to demonstrate that there are no nanoparticles deposited in the vicinity of contact line region during the dynamic wetting. If the self-assembly of nanoparticles occurs in the vicinity of contact line region, the contact line will move on the "SiO_2 solid surfaces," no matter what the substrate is; thus, the value of ζ for glass, silicon, and mica slides should equal with each other. The different ζ indicates that the self-assembly of nanoparticles does not occurs. The results provide an indirect evidence to confirm that the dilute nanofluid dynamic wetting is dominated by the bulk dissipation.

2.3.4.3 Newtonian Dynamic Wetting Behaviors of Dilute Nanofluids

It is restated that the 1/10 spreading exponent is derived from the hydrodynamics model for the Newtonian dynamic wetting. Thus, the dynamic wetting of dilute nanofluids behaves like that of Newtonian fluids, which is further confirmed by measuring the rheological properties of nanofluids with four nanoparticle loadings (PDMS500, SiO_2 with φ = 0, 0.5, 1, and 2 %, d = 20 nm), as shown in Fig. 2.15. There is still a debate about whether nanofluids exhibit Newtonian or non-Newtonian behavior [42–48]. Chen et al. [49] and Yu et al. [50] stated that the

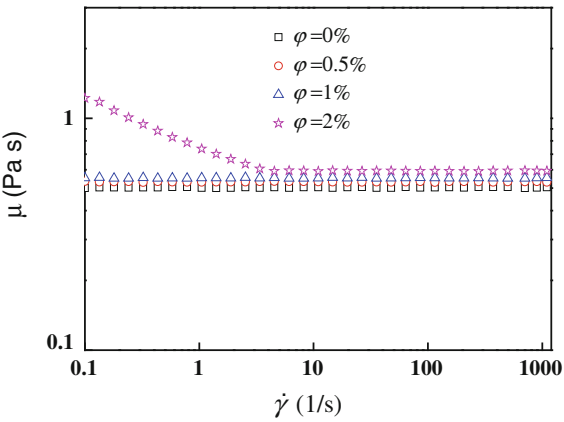

Fig. 2.15 Relation of dynamic viscosity versus shear rate for nanofluids with four nanoparticle loadings (SiO_2, PDMS500, φ = 0, 0.5, 1, and 2 %, d = 20 nm)

Newtonian or non-Newtonian rheology of nanofluids depends strongly on the nanoparticle volume fraction. The volume-fraction-dependent rheology of nanofluids was explained on the molecular level by considering the effects of the nanoparticle motion and aggregation [40]. In Wang et al.'s work [13, 14], the mass fraction of silica nanoparticles in PPG was 7.5 and 10 %, far higher than the present loadings, which leads to the shear-thickening rheology and hence to the shear-thickening dynamic wetting behavior. However, for the present dilute nanofluids, the nanoparticles distribute uniformly in the bulk liquid. This homogeneous nanoparticle distribution reduces the nanoparticle aggregation in the bulk liquid, leading to the Newtonian-like dynamic wetting behavior.

2.4 Conclusions

The variations of wetting radius and contact angle with time were measured using the droplet spreading method to study the dynamic wetting behaviors of dilute nanofluids. Various effects, such as the nanoparticle material, loading, and diameter, the base fluid, and the substrate, were considered in this study. The main conclusions are as follows.

1. The nanoparticles inhibit rather than facilitate the dynamic wetting of dilute nanofluids. Both the contact line velocity and the spreading area decrease with increasing loading. The individual parameter analysis shows that the deterioration in dynamic wetting for dilute nanofluids can be attributed to the increase in either surface tension or viscosity due to adding nanoparticles into the base fluid.
2. The spreading exponent fitted from the nanofluid dynamic wetting data is found to be very close to 0.1, which meets the prediction of the classical hydrodynamics model derived from bulk viscous dissipation approach for Newtonian

flows. This is because the nanoparticles in dilute nanofluids are uniformly distributed in the bulk liquid. The homogeneous nanoparticle distribution reduces the nanoparticle aggregation in the bulk liquid and the self-assembly in the contact line region, leading to a Newtonian-like dynamic wetting behavior.
3. It is interesting that once the effects of the surfaces tension and viscosity are both eliminated using the non-dimensional analysis, the wetting radius versus spreading time (R–t) curves for all the nanofluid droplets overlap with each other. This result and the Newtonian-like behavior demonstrate that the dynamic wetting of dilute nanofluids is dominated by the bulk dissipation.

The present results provide a better understanding and direct evidences of the bulk dissipation mechanism for the dilute nanofluid dynamic wetting. The finding of Newtonian-like behavior in dilute nanofluids also provides a guideline for building theoretical models of the dynamic wetting of dilute nanofluids.

References

1. Chakraborty S, Padhy S (2008) Anomalous electrical conductivity of nanoscale colloidal suspensions. ACS Nano 2:2029–2036
2. Trisaksri V, Wongwises S (2007) Critical review of heat transfer characteristics of nanofluids. Renew Sust Energ Rev 11:512–523
3. Branson BT, Beauchamp PS, Beam JC et al (2013) Nanodiamond nanofluids for enhanced thermal conductivity. ACS Nano 7:3183–3189
4. Choi SUS (1995) Enhancing thermal conductivity of fluids with nanoparticles. In: Developments and application of non-newtonian flows. ASME, New York
5. Choi SUS (2009) Nanofluids: from vision to reality through research. J Heat Transfer 131:033106–033111
6. Cheng LS, Cao DP (2011) Designing a thermo-switchable channel for nanofluidic controllable transportation. ACS Nano 5:1102–1108
7. Michaelides EE (2013) Transport properties of nanofluids. A critical review. J Non-Equilib Thermodyn 38:1–79
8. Moosavi M, Goharshadi EK, Youssefi A (2010) Fabrication, characterization, and measurement of some physicochemical properties of ZnO nanofluids. Int J Heat Mass Transfer 31:599–605
9. Tanvir S, Li Q (2012) Surface tension of nanofluid-type fuels containing suspended nanomaterials. Nanoscale Res Lett 7:226–236
10. Vafaei S, Purkayastha A, Jain A (2009) The effect of nanoparticles on the liquid-gas surface tension of Bi_2Te_3 nanofluids. Nanotechnology 20:185702
11. Chen HS, Ding YL, Lapkin A (2009) Rheological behaviour of nanofluids containing tube rod-like nanoparticles. Powder Tech 194:132–141
12. Lee YS, Wagner NJ (2003) Dynamic properties of shear thickening colloidal suspensions. Rheol Acta 42:199–208
13. Wang XD, Lee DJ, Peng XF et al (2007) Spreading dynamics and dynamic contact angle of non-Newtonian fluids. Langmuir 23:8042–8047
14. Wang XD, Zhang Y, Lee DJ (2007) Spreading of completely wetting or partially wetting power-law fluid on solid surface. Langmuir 23:9258–9262
15. Wasan DT, Nikolov AD (2003) Spreading of nanofluids on solids. Nature 423:156–159

16. Kondiparty K, Nikolov AD, Wu S (2011) Wetting and spreading of nanofluids on solid surfaces driven by the structural disjoining pressure: statics analysis and experiments. Langmuir 27:3324–3335
17. Kondiparty K, Nikolov AD, Wasan DT et al (2012) Dynamic spreading of nanofluids on solids. Part I: experimental. Langmuir 28:14618–14623
18. Liu KL, Kondiparty K, Nikolov AD et al (2012) Dynamic spreading of nanofluids on solids. Part II: modeling. Langmuir 28:16274–16284
19. Sefiane K, Bennacer R (2009) Nanofluids droplets evaporation kinetics and wetting dynamics on rough heated substrates. Adv Colloid Interface Sci 147–148:263–271
20. Moffat JR, Sefiane K, Shanahan MER (2009) Effect of TiO_2 nanoparticles on contact line stick-slip behavior of volatile drops. J Phys Chem B 113:8860–8866
21. Murshed SMS, Nieto de Castro CA, Lourenco MJV et al (2007) A review of boiling and convective heat transfer with nanofluids. Renew Sust Energy Rev 15:2342–2354
22. Wen DS (2008) Mechanisms of thermal nanofluids on enhanced critical heat flux (CHF). Int J Heat Mass Transfer 51:4958–4965
23. Kim SJ, Bang IC, Buongiorno J et al (2006) Effects of nanoparticle deposition on surface wettability influencing boiling heat transfer in nanofluids. Appl Phys Lett 89:153107
24. Sefiane K (2006) On the role of structural disjoining pressure and contact line pinning in critical heat flux enhancement during boiling of nanofluids. Appl Phys Lett 89:044106
25. Sefiane K, Skilling J, MacGillivary J (2008) Contact line motion and dynamic wetting of nanofluid solutions. Adv Colloid Interface Sci 138:101–120
26. Liang ZP, Wang XD, Lee DJ et al (2009) Spreading dynamics of power-law fluid droplets. J Phys Condens Matter 21:464117
27. Lu G, Hu H, Duan YY et al (2013) Wetting kinetics of water nano-droplet containing non-surfactant nanoparticles: a molecular dynamics study. Appl Phys Lett 103:253104
28. Huh C, Mason SG (1977) Steady movement of a liquid meniscus in a capillary tube. J Fluid Mech 81:401–419
29. Dussan VEB (1976) The moving contact line: the slip boundary conditions. J Fluid Mech 76:665–684
30. Tanner LH (1979) The spreading of silicone oil drops on horizontal surfaces. J Phys D 12:1473–1484
31. Blake TD, Haynes JM (1969) Kinetics of liquid/liquid displacement. J Colloid Interface Sci 30:421–423
32. Nicolas M (2005) Spreading of a drop of neutrally buoyantsuspension. J Mech Fluid 545:271–280
33. Chandrasekar M, Suresh S, Chandra BA (2010) Experimental investigations and theoretical determination of thermal conductivity and viscosity of Al_2O_3/water nanofluids. Exp Thermal Fluid Sci 34:210–216
34. Nguyen CT, Desgranges F, Galanis N et al (2008) Viscosity data for Al_2O_3-water nanofluid-hysteresis: is heat transfer enhancement using nanofluids reliable. Int J Therm Sci 47:103–111
35. Lee JH, Hwang KS, Janga S et al (2008) Effective viscosities and thermal conductivities of aqueous nanofluids containing low volume concentrations of Al_2O_3 nanoparticles. Int J Heat Mass Transfer 51:2651–2656
36. Prasher R, Song D, Wang J et al (2006) Measurements of nanofluid viscosity and its implications for thermal applications. Appl Phys Lett 89:133108–133111
37. Murshed SM, Tan SH, Nguyen NT (2008) Temperature dependence of interfacial properties and viscosity of nanofluids for droplet-based microfluidics. J Phys D Appl Phys 41:085502
38. Radiom M, Yang C, Chan WK (2010) Characterization of surface tension and contact angle of nanofluids. Proc SPIE 7522:75221D
39. Liu Y, Kai D (2012) Investigations of surface tension of binary nanofluids. Adv Mater Res 347–353:786–790
40. Lu G, Duan YY, Wang XD (2014) Surface tension, viscosity, and rheology of water-based nanofluids: a microscopic interpretation on the molecular level. J Nanopart Res 16:2564

41. Chen P (2005) Molecular interfacial phenomena of polymers and biopolymers. In: Grundke K (ed) Surface-energetic properties of polymers in controlled architecture. Woodhead, Cambridge, pp 323–374
42. Chen HS, Ding YL, He YR et al (2007) Rheological behaviour of ethylene glycol based titania nanofluids. Chem Phys Lett 444:333–337
43. Susan-Resiga D, Socoliuc V, Boros T et al (2012) The influence of particle clustering on the rheological properties of highly concentrated magnetic nanofluids. J Colloid Interface Sci 373:110–115
44. Wang XW, Xu XF, Choi SUS (1999) Thermal conductivity of nanoparticle-fluid mixture. J Thermophys Heat Transfer 13:474–480
45. Chen HS, Ding YL, Lapkin A (2009) Rheological behaviour of nanofluids containing tube rod-like nanoparticles. Powder Technol 194:132–141
46. Ding Y, Alias H, Wen D et al (2006) Heat transfer of aqueous suspensions of carbon nanotubes (CNT nanofluids). Int J Heat Mass Transfer 49:240–250
47. Kole M, Dey TK (2011) Effect of aggregation on the viscosity of copper oxide-gear oil nanofluids. Int J Thermal Sci 50:1741–1747
48. Kim S, Kim C, Lee WH et al (2011) Rheological properties of alumina nanofluids and their implication to the heat transfer enhancement mechanism. J Appl Phys 110:34316
49. Chen HS, Ding YL, Tan CQ (2007) Rheological behaviour of nanofluids. New J Phys 9:367
50. Yu W, Xie H, Chen L et al (2009) Investigation of thermal conductivity and viscosity of ethylene glycol based ZnO nanofluids. Thermo Chimica Acta 491:92–99

http://www.springer.com/978-3-662-48763-1

Dynamic Wetting by Nanofluids

Lu, G.

2016, XIII, 112 p. 75 illus., 2 illus. in color., Hardcover
ISBN: 978-3-662-48763-1